# $^{90}$Y Bremsstrahlung Imaging for Absorbed-Dose Assessment in High-Dose Radioimmunotherapy

David Minarik[1], Katarina Sjögreen-Gleisner[1], Ola Linden[2], Karin Wingårdh[1,2], Jan Tennvall[2], Sven-Erik Strand[1], and Michael Ljungberg[1]

[1]Department of Medical Radiation Physics, Clinical Sciences, Lund University, Lund, Sweden; and [2]Department of Oncology, Lund University and Skåne University Hospital, Lund, Sweden

This feasibility study demonstrates $^{90}$Y quantitative bremsstrahlung imaging of patients undergoing high-dose myeloablative $^{90}$Y-ibritumomab treatment. **Methods:** The study includes pretherapy $^{111}$In SPECT/CT and planar whole-body (WB) imaging at 7 d and therapy $^{90}$Y SPECT/CT at 6 d and $^{90}$Y WB imaging at 1 d. Time–activity curves and organ-absorbed doses derived from $^{90}$Y SPECT images were compared with pretherapy $^{111}$In estimates. Organ activities derived from $^{90}$Y WB images at the first day were compared with corresponding pretherapy estimates. **Results:** Pretherapy $^{111}$In images from 3 patients were similar to the $^{90}$Y images. Differences between absorbed-dose estimates from pretherapy $^{111}$In and $^{90}$Y therapy were within 25%, except for the lungs. Corresponding activity differences derived from WB images were within 25%. Differences were ascribed to incomplete compensation methods and real differences in pharmacokinetics between pretherapy and therapy. **Conclusion:** Quantitative bremsstrahlung imaging to estimate organ activities and absorbed doses is feasible.

**Key Words:** yttrium; bremsstrahlung; imaging; radioimmunotherapy; activity quantification

R adioimmunotherapy is established for the treatment of relapsing follicular or transformed B-cell lymphomas. Two radioimmunoconjugates, $^{90}$Y-ibritumomab (Zevalin; Spectrum Pharmaceuticals) and $^{131}$I-tositumomab (Bexxar; GlaxoSmithKline), were approved. A dose–response relationship can be inferred from several observations (1,2), and the best clinical results published have made use of myeloablative radioimmunotherapy (3).

In standard $^{90}$Y-ibritumomab treatments, administered activity is based on patient weight. For high-dose ibritumomab studies involving bone-marrow stem-cell support, an accurate dosimetry is required. The organs at risk in these studies are the liver, kidneys, and lungs. To maximize the

therapy effect, it is important to not exceed the maximum-tolerable dose (MTD). We have an ongoing clinical absorbed dose–escalation study to determine MTD for the liver based on a pretherapy dose planning. The pretherapy dosimetry is performed by imaging with $^{111}$In-labeled ibritumomab to predict the $^{90}$Y activity required for treatment. There is also a need to monitor the actual treatment for dose verification. A mixture of $^{111}$In- and $^{90}$Y-labeled ibritumomab could allow for imaging; however, this method has potential drawbacks. First, any labeling instability produces free-circulating $^{111}$In, which gives nonrepresentative image information. Second, $^{90}$Y bremsstrahlung may contaminate the $^{111}$In energy windows, leading to errors in the activity quantification. Third, an $^{111}$In-ibritumomab kit can be costly. If quantitative $^{90}$Y bremsstrahlung imaging is feasible, such a study could confirm both targeting and delivery of the prescribed absorbed dose.

Previously, we have experimentally investigated quantitative bremsstrahlung SPECT and planar whole-body (WB) imaging (4,5). To our knowledge, no studies have been performed on quantitative bremsstrahlung imaging of patients given radiolabeled monoclonal antibody. In this work, the feasibility of quantitative bremsstrahlung imaging to verify predicted absorbed doses was investigated for SPECT and WB imaging using data from our escalation study. That study includes a pretherapy study with $^{111}$In-labeled ibritumomab in which SPECT/CT and WB imaging allow for a comparison of quantitative $^{90}$Y with quantitative $^{111}$In imaging.

## MATERIALS AND METHODS

### Patients and Study Protocol

In this work, 3 patients were evaluated (2 men [ages, 74 and 57 y; weights, 74 and 79 kg] and 1 woman [age, 71 y; weight, 70 kg]). The organ at risk was the liver, because bone-marrow stem-cell support was given. All patients received 300 MBq of $^{111}$In-ibritumomab in the pretherapy study, followed by SPECT/CT and WB imaging on 7 occasions (at 1, 24, 48, 72, 144, 166, and 192 h after imaging). The SPECT/CT data determined the necessary therapy activity to give 12 Gy to the liver, and the WB studies served as an independent activity-quantification method to confirm the SPECT dosimetry. The $^{90}$Y activities were calculated to 2,915, 4,990, and 1,825 MBq. Before $^{90}$Y infusion, all patients received cold rituximab. The therapy study included 6 measurements at 1,

24, 48, 120, 144, and 166 h after injection. Both SPECT/CT and WB images were acquired on the first occasion, but only SPECT/CT measurements were performed on the other 5 occasions.

## Imaging System

A SPECT/CT Discovery VH system (GE Healthcare), equipped with 2.54-cm NaI(TI) crystals and a Hawkeye CT, was used. [111]In images were acquired from two 15% energy windows centered over the 245- and 172-keV peaks. A medium-energy general-purpose collimator was used for ^{111}In imaging, and ^{90}Y images were acquired using a high-energy general-purpose collimator and a 60% energy window centered at 150 keV. Anterior and posterior WB images were acquired in 384 × 1,024 matrices, with a pixel size of 2.21 mm. The scan speed was 20 cm/min for the first 3 measurements in the pretherapy study and 10 cm/min for all other measurements. SPECT data were acquired in a 64 × 64 matrix for 60 projections and 360°. For each time point, a CT study was conducted. The acquisition times per SPECT projection for ^{111}In and ^{90}Y were 45 and 60 s, respectively. All images were processed using the LundADose software (6). The system sensitivities were measured from a known activity in air for ^{111}In and behind a 10-mm clear acrylic sheet for ^{90}Y and were 72, 12, 1, and 0.16 cps/MBq for ^{111}In SPECT, ^{111}In WB, ^{90}Y SPECT, and ^{90}Y WB imaging, respectively.

## SPECT Activity Quantification

SPECT images were reconstructed with an iterative ordered-subset expectation maximization algorithm (7) using 6 angles per subset. Attenuation correction was made using a CT-based density map (8) scaled to proper photon energy, with either soft-tissue– or bone-equivalent mass-attenuation coefficients, depending on a threshold of 1.2 g·cm$^{-3}$. Scatter was modeled using the effective source scatter estimation (9) including compensation for the collimator–detector response. Both effective source scatter estimation and collimator–detector response kernels were generated from Monte Carlo simulations (10). The ^{111}In images were reconstructed using 6 iterations and the ^{90}Y images using 3 iterations. The mean organ activity concentration was calculated from volumes of interest delineated with sufficient margins to avoid partial-volume effects.

## Planar Activity Quantification

Organ activities were quantified using a pixel-based conjugate-view method (4,6). A patient-specific narrow-beam attenuation map was determined from an x-ray scout image (11) to correct for attenuation. To scale the map to the ^{90}Y energy window, energy abundance–weighted linear attenuation coefficients were calculated from bremsstrahlung emission spectra obtained using MCNPX (12). Because of the 40-cm difference between the camera heads and x-ray unit, the patients were repositioned between the emission and scout scans. A software-based image registration, based on mutual information between the geometric mean–averaged WB image and the scout image (13,14), was applied for a correct pixel-based attenuation correction (15). The spatial change included the transformation of regions covering the head, torso, and left and right legs and was based on second-degree polynomials with translation, rotation, shearing, and second-degree curving included (15). Compensation for scatter, collimator response, and counts from backscattered photons was applied (4).

Organ activities were calculated from regions of interest (ROIs), and corrections for background activity and overlapping activities were made on a pixel basis in the activity images (16).

## Absorbed-Dose Calculation and Evaluation

SPECT ^{90}Y images were evaluated by comparing ^{111}In and ^{90}Y SPECT–based time–activity curves and absorbed doses for the liver, spleen, kidneys, and lungs. Differences in administered activities, half-lives, and times were considered by renormalizing the ^{111}In activity, $A_{In}$:

$$A_{In \,->Y} = A_{In} \cdot e^{(\lambda_{In} - \lambda_Y) \cdot t} \cdot \frac{A_{o,Y}}{A_{o,In}}, \qquad \text{Eq. 1}$$

where $\lambda$ represents the decay constant, $A_o$ the administered activity, and $t$ the time between infusion and imaging. Organ time–activity curves were calculated by a biexponential fit using Levenberg–Marquardt least-squares minimization of the $\chi^2$ statistical metric. Organ-absorbed doses were calculated by multiplying the cumulated activity concentration (MBq·h/cm$^3$) by the emitted energy per megabecquerel divided by the mass density. The kinetic energy was assumed locally absorbed, because the range of the β-particles from ^{90}Y are comparable to the SPECT spatial resolution.

Planar WB ^{90}Y images were evaluated by comparing ^{111}In and ^{90}Y activities in the liver, spleen, kidneys, lungs, and total body, for which ^{111}In images were normalized as:

$$A_{In \,->Y} = A_{In} \cdot e^{\lambda_{In} \cdot t_{In} - \lambda_Y \cdot t_Y} \cdot \frac{A_{o,Y}}{A_{o,In}}, \qquad \text{Eq. 2}$$

where $t_{In}$ and $t_Y$ are the elapsed times between infusion and first measurement for pretherapy and therapy, respectively.

## RESULTS

### SPECT

Figure 1 shows time–activity curves for patient 1. The ^{90}Y time–activity curve for the liver is consistent with the ^{111}In time–activity curve, apart from the first time point. The spleen time–activity curves differ somewhat between ^{111}In and ^{90}Y, showing a slightly lower initial uptake for [90]Y. The ^{111}In and ^{90}Y time–activity curves for the kidneys correspond well, and the left and right kidneys exhibit almost identical kinetics. For the lungs, the ^{90}Y time–activity curves are elevated, compared with the ^{111}In time–activity curve, but the kinetics for the left and right lungs are similar.

Table 1 shows calculated organ-absorbed doses. For the liver, organ-absorbed doses agreed well for patients 1 and 3, but for patient 2 the absorbed-dose calculated from ^{90}Y images was 25% higher than that estimated from ^{111}In images. The spleen values were within 20% for patients 1 and 2 and within 30% for patient 3, and the kidney values were within 14%. Considerable differences were seen in the absorbed doses to the lungs.

Figure 2 shows SPECT images through the liver and spleen for ^{111}In and ^{90}Y for patient 1. It is evident that the ^{111}In images have better spatial resolution and image contrast. However, the ^{90}Y images compare well with ^{111}In images, despite apparent background and nonuniform organ boundaries.

### WB Imaging

Table 2 summarizes activity estimates based on the planar ^{111}In images and ^{90}Y images. Figure 3 demonstrates the
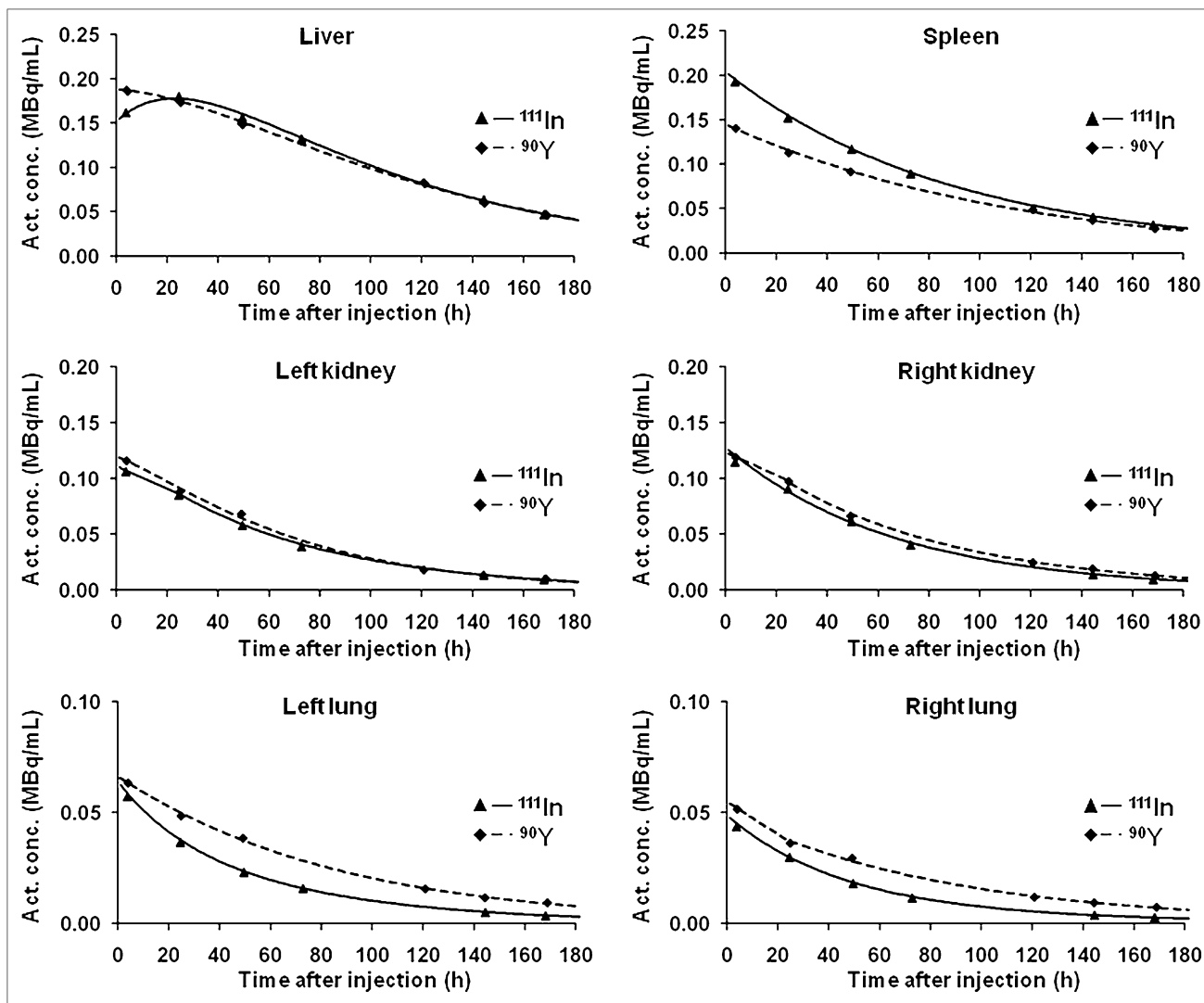
**FIGURE 1.** Mean activity concentration in liver, spleen, kidneys, and lungs calculated from SPECT for patient 1. Act. conc. = activity concentration.

improvement in image quality from the restoration filtering and the quantitative procedure. The ROIs used to quantify both the ^{111}In and the ^{90}Y images are also displayed. For all patients and organs, the differences in activities obtained from the ^{90}Y images and from ^{111}In imaging are within 25%. Estimated total-body activities, compared with the administered activities, showed deviations of −7%, −5%, and −7% for the ^{111}In-based estimates and 9%, 5%, and

**TABLE 1**
Absorbed Doses to Organs, Calculated from SPECT Images

| Organ | Patient 1 | | | Patient 2 | | | Patient 3 | | |
|---|---|---|---|---|---|---|---|---|---|
| | [90]Y | [111]In | % | [90]Y | [111]In | % | [90]Y | [111]In | % |
| Liver | 12.1 | 12.1 | 0.0 | 14.7 | 11.8 | 24.6 | 10.8 | 11.0 | −1.8 |
| Spleen | 7.5 | 9.3 | −19.4 | 15.0 | 13.1 | 14.5 | 5.8 | 4.5 | 28.9 |
| Left kidney | 4.6 | 4.1 | 12.2 | 8.7 | 8.0 | 8.7 | 2.8 | 3.1 | −9.7 |
| Right kidney | 5.0 | 4.4 | 13.6 | 8.4 | 8.2 | 2.4 | 3.3 | 3.1 | 6.5 |
| Left lung | 10.5 | 6.4 | 64.1 | 13.5 | 11.1 | 21.6 | 9.1 | 5.6 | 62.5 |
| Right lung | 8.1 | 4.9 | 65.3 | 12.2 | 9.1 | 34.1 | 7.8 | 4.8 | 62.5 |

Corresponding ^{90}Y-absorbed doses were calculated from ^{111}In images using Equation 1. Percentages were calculated by ([90]Y − [111]In)/[111]In × 100%.
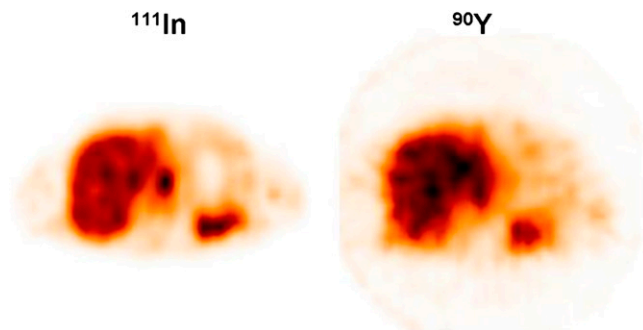
**FIGURE 2.** $^{111}$In and $^{90}$Y images from patient 1 at first time point.

8% for the $^{90}$Y-based estimates for patients 1, 2, and 3, respectively.

## DISCUSSION

The feasibility of clinical quantitative bremsstrahlung imaging has been investigated by comparing absorbed doses calculated from multiple SPECT/CT scans of $^{111}$In-labeled ibritumomab acquired before therapy with those acquired during therapy with $^{90}$Y-ibritumomab. The activities obtained from WB $^{111}$In images and planar WB $^{90}$Y images have also been compared.

The difference between the $^{111}$In and $^{90}$Y time–activity curves (Fig. 1), the corresponding absorbed-dose estimates, and the planar WB activities were mostly of the same magnitude for all patients. There were some differences that could be related to measurement uncertainties or actual differences in pharmacokinetics. Regarding the liver, the absorbed doses corresponded well for patients 1 and 3. For patient 1, a slightly higher activity was obtained for the $^{90}$Y-based estimation at the first SPECT measurement, and a similar difference was seen for the WB-derived value. For this patient, there could be a difference in the actual uptake because the pretherapy study was performed 4 mo before therapy. The $^{90}$Y liver time–activity curve, compared with the $^{111}$In time–activity curve, for patient 2 (not shown) was elevated, and the absorbed dose to the liver was estimated to be 14.7 Gy from the $^{90}$Y time–activity curve but

only 11.8 Gy from the $^{111}$In extrapolation. The reason for the 24.6% difference is not yet understood. For patient 3, the liver time–activity curves and absorbed doses were in good agreement. The 11 Gy estimated from the $^{111}$In images was based on the actual amount of delivered $^{90}$Y activity and therefore deviates from the prescribed 12 Gy.

For all patients, the difference in the absorbed dose before therapy and during therapy was larger for the spleen than for the liver and kidneys. The spleen is relatively small, and size differs between the patients. Partial-volume effects could therefore influence the estimates differently between the patients. The kidneys are also relatively small, but $^{111}$In- and $^{90}$Y-derived kidney absorbed doses were similar for all patients. The differences for the spleen could therefore be interpreted as a real difference in uptake. The washout rate for patient 1 (Fig. 1) seems similar, but the initial uptake is slightly lower for the therapeutic infusion. Generally, the spleen can be regarded as a target organ, and the number of available binding sites of the antigen CD20 before therapy and during therapy can differ because of the infusion of cold monoclonal antibody.

For the lungs, the $^{90}$Y time–activity curves, compared with the $^{111}$In time–activity curves, were generally elevated, with corresponding absorbed-dose deviations up to 65%. These deviations may relate to insufficient compensation methods. A bremsstrahlung image has a more diffuse background with a higher intensity than an $^{111}$In image (Fig. 3). Most counts seen outside the patient boundary in Figure 3A stem from photons that have scattered in or penetrated the septa, passed the crystal, and then backscattered. This scatter background, combined with the fact that lungs are located between organs with elevated uptake (liver and blood in the heart), could explain some of the obtained differences. The effective source scatter estimation kernels are invariant regarding density, and the method is therefore not expected to be accurate in areas with heterogeneous attenuation.

Total-body activities, compared with administered activities, from WB $^{90}$Y images were approximately 10% higher than corresponding $^{111}$In estimates—on average 7%. There

**TABLE 2**
Organ Activities at 1 Hour After injection, Calculated from WB Images

| Organ | Patient 1 | | | Patient 2 | | | Patient 3 | | |
|---|---|---|---|---|---|---|---|---|---|
| | $^{90}$Y | $^{111}$In | % | $^{90}$Y | $^{111}$In | % | $^{90}$Y | $^{111}$In | % |
| Total body | 3,180 | 2,831 | 12 | 5,243 | 4,755 | 10 | 1,979 | 1,689 | 17 |
| Liver | 243.5 | 220.0 | 10.7 | 488.1 | 451.6 | 8.1 | 221.9 | 243.3 | −8.8 |
| Spleen | 25.8 | 26.2 | −1.6 | 140.2 | 187.2 | −25.1 | 63.8 | 59.1 | 8.0 |
| Left kidney | 36.1 | 38.7 | −6.7 | 76.1 | 82.7 | −8.0 | 31.6 | 27.4 | 15.3 |
| Right kidney | 26.4 | 30.5 | −13.5 | 57.8 | 55.9 | 3.5 | 24.7 | 25.0 | 0.0 |
| Left lung | 87.6 | 91.4 | −4.1 | 135.6 | 173.4 | −21.8 | 40.5 | 54.0 | −24.9 |
| Right lung | 94.5 | 106.5 | −11.2 | 173.5 | 195.9 | −11.4 | 41.9 | 55.7 | −24.7 |

Corresponding $^{90}$Y activity was calculated from $^{111}$In images using Equation 2. Percentages were calculated by ($^{90}$Y − $^{111}$In)/$^{111}$In × 100%.
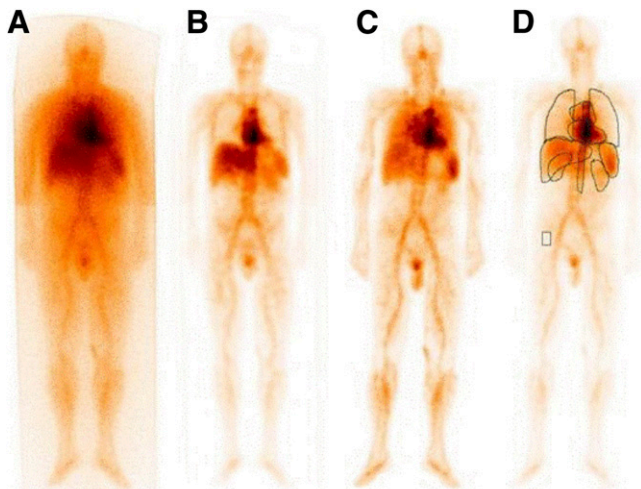
**FIGURE 3.** Unprocessed (A) and processed (B) $^{90}$Y WB images and corresponding unprocessed (C) and processed (D) $^{111}$In images. Curvature comes from registration process. ROIs used are shown in D.

are 2 reasons for this. First, the mean energy of the bremsstrahlung image in the 105- to 195-keV energy interval is about 140 keV, which means that the overestimation that arises from the source thickness when applying the geometric mean is larger for $^{90}$Y. Second, the diffuse background in $^{90}$Y images is difficult to correct for. It has been found that organ activities based on WB studies can be underestimated by a few percentage points (*4*). Also for this study, the $^{90}$Y activity estimates were often lower than $^{111}$In estimates, contrary to results from SPECT. These lower estimates were especially evident for the lungs, for which $^{90}$Y activity concentration from SPECT estimates for the first time point were between 10% and 25% higher than the $^{111}$In-based estimates. The planar-based $^{90}$Y activity estimates were up to 20% lower than the $^{111}$In-based estimates. Generally, for the $^{111}$In and $^{90}$Y measurements at the first time point the WB estimates deviated by the same order of magnitude as the SPECT estimates. However, conjugate-view quantification may be more prone to variation because it is sensitive to subjective actions such as defining ROIs.

## CONCLUSION

This work shows that adequate compensations for attenuation, scatter, and collimator response make $^{90}$Y bremsstrahlung imaging feasible, with a relatively good image quality and useful quantitative accuracy. These compensations may be of great importance for absorbed-dose planning of high-dose radioimmunotherapy and for future improved dosimetry protocols for present $^{90}$Y-based radionuclide therapies, such as standard $^{90}$Y-ibritumomab treatment.

## REFERENCES

1. Du Y, Honeychurch J, Cragg MS, et al. Antibody-induced intracellular signaling works in combination with radiation to eradicate lymphoma in radioimmunotherapy. *Blood.* 2004;103:1485–1494.
2. Koral KF, Francis IR, Kroll S, Zasadny KR, Kaminski MS, Wahl RL. Volume reduction versus radiation dose for tumors in previously untreated lymphoma patients who received iodine-131 tositumomab therapy: conjugate views compared with a hybrid method. *Cancer.* 2002;94(4, suppl):1258–1263.
3. Liu SY, Eary JF, Petersdorf SH, et al. Follow-up of relapsed B-cell lymphoma patients treated with iodine-131-labeled anti-CD20 antibody and autologous stem-cell rescue. *J Clin Oncol.* 1998;16:3270–3278.
4. Minarik D, Ljungberg M, Segars P, Gleisner KS. Evaluation of quantitative planar $^{90}$Y bremsstrahlung whole-body imaging. *Phys Med Biol.* 2009;54: 5873–5883.
5. Minarik D, Sjogreen GK, Ljungberg M. Evaluation of quantitative $^{90}$Y SPECT based on experimental phantom studies. *Phys Med Biol.* 2008;53:5689–5703.
6. Sjogreen K, Ljungberg M, Wingardh K, Minarik D, Strand SE. The LundADose method for planar image activity quantification and absorbed-dose assessment in radionuclide therapy. *Cancer Biother Radiopharm.* 2005;20:92–97.
7. He B, Du Y, Song X, Segars WP, Frey EC. A Monte Carlo and physical phantom evaluation of quantitative In-111 SPECT. *Phys Med Biol.* 2005;50: 4169–4185.
8. Sjogreen-Gleisner K, Rueckert D, Ljungberg M. Registration of serial SPECT/ CT images for three-dimensional dosimetry in radionuclide therapy. *Phys Med Biol.* 2009;54:6181–6200.
9. Frey EC, Tsui BMW. A new method for modeling the spatially-variant, object-dependent scatter response function in SPECT. *IEEE Nuclear Science Symposium.* 1996;2:1082–1086.
10. Ljungberg M, Strand SE. A Monte Carlo program for the simulation of scintillation camera characteristics. *Comput Methods Programs Biomed.* 1989;29:257–272.
11. Minarik D, Sjogreen K, Ljungberg M. A new method to obtain transmission images for planar whole-body activity quantification. *Cancer Biother Radiopharm.* 2005;20:72–76.
12. Hendricks JS. *MCNPX, Version 2.6.A.* Vol. LA-UR-05-8225. Los Alamos, NM: Los Alamos National Laboratory; 2005.
13. Maes F, Collignon A, Vandermeulen D, Marchal G, Suetens P. Multimodality image registration by maximization of mutual information. *IEEE Trans Med Imaging.* 1997;16:187–198.
14. Wells WM III, Viola P, Atsumi H, Nakajima S, Kikinis R. Multi-modal volume registration by maximization of mutual information. *Med Image Anal.* 1996;1: 35–51.
15. Sjogreen K, Ljungberg M, Wingardh K, Erlandsson K, Strand SE. Registration of emission and transmission whole-body scintillation-camera images. *J Nucl Med.* 2001;42:1563–1570.
16. Sjogreen K, Ljungberg M, Strand SE. An activity quantification method based on registration of CT and whole-body scintillation camera images, with application to $^{131}$I. *J Nucl Med.* 2002;43:972–982.